Hindawi
Advances in Civil Engineering
Volume 2020, Article ID 6694180, 11 pages
https://doi.org/10.1155/2020/6694180

Research Article

Finite Element (FE) Modeling of Indirect Tension to Cylindrical (IT-CY) Specimen Test for Damping Asphalt Mixtures (DAMs)

Jiandong Huang,[1,2] Tianhong Duan ,[1,2] Yuantian Sun ,[1,2] Lin Wang,[2] and Yawei Lei[3]

[1]*State Key Laboratory of Coal Resources and Safe Mining, China University of Mining and Technology, Xuzhou 221116, China*
[2]*School of Mines, China University of Mining and Technology, Xuzhou 221116, China*
[3]*China Construction Second Engineering Bureau Ltd., Beijing 100160, China*

Correspondence should be addressed to Tianhong Duan; passionduan@cumt.edu.cn and Yuantian Sun; yuantiansun@cumt.edu.cn

Received 3 November 2020; Revised 24 November 2020; Accepted 27 November 2020; Published 21 December 2020

Academic Editor: Jiaolong Ren

DAMs have recently been developed to be used as the damping layer in the so-called antivibration pavement to mitigate the effects of traffic-induced vibration while rare finite element (FE) modeling has been conducted to simulate the indirect tension to cylindrical (IT-CY) specimen test for DAMs. In the present study, the methods for the viscoelastic characterization of DAMs and the techniques to characterize the viscoelastic behavior of DAMs in FE modeling were proposed. The FE model to simulate the IT-CY test was constructed, and it was verified through the corresponding laboratory test. Good agreements were noted between the simulation results and testing results demonstrating that the FE model can provide the accurate prediction of the mechanical behavior of DAMs.

1. Introduction

In recent years, various indirect tensile tests of asphalt mixture have been widely used in the evaluation and design in pavement engineering [1–5]. Among these, the indirect tension to cylindrical (IT-CY) specimen test is a method for measuring the dynamic stiffness of asphalt mixtures. It can be applied to cylindrical specimens of various diameters and thickness, manufactured in the laboratory or cored from a road layer (Institution 2004) to reflect the mechanical properties of the asphaltic materials, provide the input mechanical parameters for the asphalt pavement design, and evaluate the crack resistance [6–12].

Based on these indirect tensile tests, various studies about the asphalt mixtures have been carried out in the past years[13, 14]. Christensen et al. applied the indirect tensile strength as the parameter to evaluate the antirutting performance of asphalt mixture and pointed out that the indirect tensile test can be used to determine the adhesive force and internal friction angle of the asphalt mixture [15]. Birgisson et al. employed the results of the superior performing asphalt pavement (Superpave) indirect tensile creep test to understand the impact of water damage on the fracture characteristics of the asphalt mixture [16]. The boundary element method (BEM) was also carried out for the numerical simulation to understand the micro-structure and fracture characteristic of asphalt mixture, using the indirect tensile test [17]. Kim et al. used the indirect tensile method to determine the dynamic modulus of the asphalt concrete, showing that the dynamic modulus master curves obtained by the uniaxial compression and indirect tensile tests have a good fit [18]. Abbas et al. used the discrete element method (DEM) to study the micromechanics of asphalt mixtures under different load conditions and numerically simulated the indirect tensile test under low-temperature conditions [19]. Zhang et al. studied the design parameters of the high-temperature characteristics of the asphalt mixture and carried out the indirect tensile test under different conditions, showing that the indirect tensile strength can replace Marshall stability as the parameter for pavement design [20]. Liang et al. conducted the indirect tensile test to evaluate the dynamic stiffness modulus of hard asphalt mixtures and understood the effects of gradation, binder/aggregate ratio, binder types, and testing temperature. Indirect tensile tests have also been conducted to evaluate the mechanical properties of lignin fiber

and glass fiber, rubberized asphalt mixture, warm asphalt mixture-reclaimed asphalt pavement as well as rutting resistance [4, 21–23]. It is evident that the indirect tensile test has been conducted and simulated from different perspectives in earlier studies[24–26]. However, to the authors' knowledge, rare numerical simulations for the IT-CY tests were conducted currently. On the other hand, as novel functional infrastructure materials, the damping asphalt mixtures (DAMs) have recently been developed to absorb vibration and noise caused by traffic loads [7, 27, 28]. DAMs can be used as the damping layer in the so-called antivibration pavement to mitigate the effects of traffic-induced vibration. The increase in damping of pavement materials can reduce ground vibrations into the loading area and within the corresponding surrounding region. This improvement is critical for reducing vibrations to improve the quality of life and to preserve the stability of buildings [29]. It has been confirmed that DAMs showed the strength to meet the requirements of the specification and had sufficient resistance to rutting and water damage [28]. However, in the case of DAMs, the IT-CY test has not been carried out in the laboratory, and the corresponding FE simulation has never been carried out in the past studies.

2. Research Objectives

The main aim of this research is to use the finite element (FE) modeling techniques to understand the mechanical behavior of DAMs in IT-CY tests. The detailed research objectives are as follows:

(i) To propose the methods for viscoelastic characterization of DAMs and the techniques to characterize the viscoelastic behavior of DAMs in FE modeling

(ii) To establish a reliable finite element (FE) model to simulate the IT-CY test and verify it through the corresponding laboratory test

(iii) To design DAMs in the laboratory, conduct IT-CY tests to characterize the viscoelastic mechanical behavior, and determine the reliable input material parameters for FE modeling

3. Methodologies

3.1. Viscoelastic Characterization of Asphalt Mixtures. As far as the constitutive model of typical viscoelastic material, like the asphalt mixtures, experimental studies have demonstrated that the viscoelastic properties can be described by the so-called generalized Maxwell model (GMM), as given in Figure 1.

The GMM consists of the restoring and viscous force components, which can be simulated by the nonlinear elastic element and the nonlinear viscous element, respectively, with these two elements connected in series [30–34]. Under the effect of constant stress, the viscous flow and deformation provided by the viscous damper can increase linearly with time, so the deformation of the whole model can increase indefinitely. Degradation of the element in the model can change this kind of mechanical characteristic, that is to say, removing a damper in one basic Maxwell model (MM).

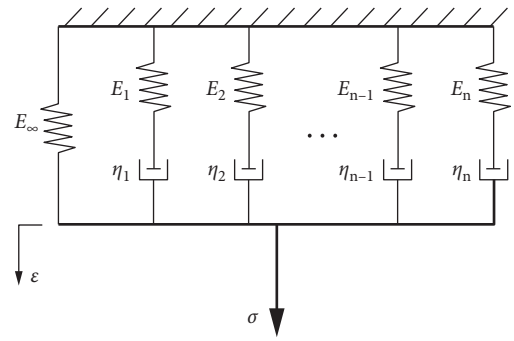

Figure 1: Generalized Maxwell model (GMM).

The constitutive model of the M-th Maxwell Model (MM) can be described as differential form:

$$\frac{d\varepsilon}{dt} = \frac{1}{E_m}\frac{d\sigma_m}{dt} + \frac{\sigma_m}{\eta_m}. \tag{1}$$

Concerning the GMM, total stress can be calculated as the sum of all MM stress:

$$\sigma = \sigma_0 + \sum_{m=1}^{M} \sigma_m. \tag{2}$$

Apply integral transformation theory and Fourier transform equations (1) and (2), respectively, under the zero initial conditions to the following equations:

$$\overline{\sigma_0} = E_0\overline{\varepsilon}, \tag{3}$$

$$\overline{\sigma_i}\left(1 + \frac{i\eta_i\omega_n}{E_i}\right) = i\omega_n\eta_i\overline{\varepsilon}, \quad n = 1, 2 \ldots N. \tag{4}$$

Substitute equations (3) and (4) into (2), and Fourier transform it as follows:

$$\overline{\sigma} = E_0\overline{\varepsilon} + \sum_{m=1}^{M} \frac{i\omega_n\eta_i}{E_i + i\eta_i\omega_n/E_i}\overline{\varepsilon}, \quad n = 1, 2, 3 \ldots N, \tag{5}$$

$$\overline{\sigma} = \overline{\varepsilon}\left(E_0 + \sum_{m=1}^{M} \frac{i\omega_n\eta_i}{1 + i\rho_i\omega_n}\right), \tag{6}$$

where $\overline{\sigma}$ and $\overline{\varepsilon}$ are complex stress and strain, respectively.

The relaxation time of the I-th MM is

$$\rho_i = \frac{\eta_i}{E_i}. \tag{7}$$

By substituting equation (7) into (6), equation (6) will be described as follows:

$$E^* = E_\infty + \sum_{m=1}^{M} \frac{i\omega_n E_i\rho_i}{1 + i\rho_i\omega_n}, \tag{8}$$

$$E^* = E_\infty + \sum_{m=1}^{M} \frac{\omega_n^2 E_i\rho_i^2}{1 + \rho_i^2\omega_n^2} + \sum_{m=1}^{M} \frac{\omega_n E_i\rho_i}{1 + \rho_i^2\omega_n^2}i. \tag{9}$$

The value of complex modulus is as follows:

$$|E^*| = \sqrt{\left(E_\infty + \sum_{m=1}^{M} \frac{\omega_n^2 E_i \rho_i^2}{1+\rho_i^2\omega_n^2}\right)^2 + \left(\sum_{m=1}^{M} \frac{\omega_n E_i \rho_i}{1+\rho_i^2\omega_n^2}\right)^2}. \quad (10)$$

3.2. Finite Element (FE) Modeling of Viscoelastic Behavior. The stress response of the viscoelastic material includes an elastic portion and a viscous portion. The elastic portion can respond immediately under the effect of load; however, the viscous portion would respond after a while. In general, the stress function of viscoelastic material is given as an integral form, and its constitutive equation may be described as follows:

$$\sigma = \int_0^t 2G(t-\tau)\frac{\mathrm{d}e}{\mathrm{d}\tau}d\tau + I\int_0^t K(t-\tau)\frac{\mathrm{d}\Delta}{\mathrm{d}\tau}\mathrm{d}\tau, \quad (11)$$

where σ is the Cauchy stress, $G(t)$ is the shear modulus function, $K(t)$ is the bulk modulus function, τ is the past time, Δ is the bulk deformation, t is the current time, and e is the shear deformation. In typical FE modeling software (e.g., ABAQUS, ANSYS, and MARC), there are two methods to describe viscoelastic integral kernel function. The first one is using GMM units by the form of Maxwell, and the second one is using the form of the Prony series. In fact, the two expression methods are consistent, and the only difference is the mathematical expression. The basic expression to describe viscoelastic properties by the Prony series is as follows:

$$G(t) = G_0\left[\alpha_\infty + \sum_{i=1}^{n} \alpha_i^G \exp\left(-\frac{t}{\tau_i^G}\right)\right], \quad (12)$$

$$K(t) = K_0\left[\alpha_\infty + \sum_{i=1}^{n} \alpha_i^K \exp\left(-\frac{t}{\tau_i^K}\right)\right], \quad (13)$$

where G_0 is the shear modulus, K_0 is the bulk modulus, and τ_i^K is the relaxation time of each Prony series. Another two parameters are defined as follows:

$$\alpha_i^G = \frac{G_i}{G_o}, \quad (14)$$

$$\alpha_i^K = \frac{K_i}{K_o}. \quad (15)$$

Besides, G_0 and K_0 could be calculated by the following functions:

$$G_0 = G(t=0) = G_\infty + \sum_{i=1}^{n} G_i, \quad (16)$$

$$K_0 = K(t=0) = K_\infty + \sum_{i=1}^{n} K_i. \quad (17)$$

Based on the viscoelastic mechanical theory, there is a relationship between these three parameters:

$$G(t) = \frac{E(t)}{2(1+\mu)}, \quad (18)$$

$$K(t) = \frac{E(t)}{3(1-2\mu)}. \quad (19)$$

Shear modulus $G(t)$ and bulk modulus $K(t)$ are unified in the same form as $E(t)$, and $E(t)$ would be expressed as a form of Prony series:

$$E(t) = E_\infty + \sum_{i=1}^{n} E_i \exp\left(-\frac{t}{\tau_i}\right). \quad (20)$$

Through the results of the experimental tests, the values of parameters in equation (10) could be fitting. By equations (18) and (19), initial and steady-state values, K_0, G_0, K_∞, and G_∞, as well as the relaxation time coefficients τ_i^G and τ_i^K can be determined.

4. Materials and Experimental Testing

4.1. Raw Materials

4.1.1. Aggregates. Basalt coarse aggregates, natural sand, and mineral filler were used for the aggregates. The physical properties were evaluated according to the EN 1097-6/7 standard, and the results are given in Table 1.

4.1.2. Binders. A plant-produced stable asphalt rubber supplied by a local manufacturer was used in the present study (ASTM D6114-97). It was produced according to the so-called wet process by mixing a Pen 50–70 base bitumen with 20% of crumb rubber, which was produced by mechanical grinding of waster scrape tires at room temperature. These scrap tires are comprised of 50% weight of truck tires and 50% weight of car tires. The gradation of the crumb rubber particles is given in Figure 2.

4.2. Mix Design. Three different rubberized open-graded asphalt mixtures are designed, which are regarded as Mix ref (mixture reference), Mix 1, and Mix 2, respectively, with the same voids in the mineral aggregate (VMA) but containing asphalt rubber content at concentrations of 5%, 15%, and 20% in order to improve the damping properties. The grain size distribution of the studied mixture respects the aggregate gradation required by the specifications for open-graded (OG) asphalt mixtures. The OG mix has been optimized and evaluated in a previous study, showing the desired mechanical properties. The nominal maximum size (NMS) of the aggregate was 8 mm, in line with the optimized design thickness of the damping layer of 3 cm [27]. The amount of binder in the mix has been increased as long as the amount of filler. Table 2 gives the passing ratio of aggregate gradation that was used in this research.

Cylindrical specimens with a diameter of 100 mm were compacted by the Superpave gyratory compactor (SGC). For mix design and all performed tests in the present study, an average of three identical samples was used as the result for

Table 1: Physical properties of aggregates (EN 1097-6/7).

Properties	Basalt	Sand	Mineral filler
Bulk specific gravity (G_{sb}) (kg/m^3)	2.753	2.629	2.710
Apparent specific gravity (G_{sa}) (kg/m^3)	2.863	2.690	2.650
Water absorption (%)	1.39	0.86	—

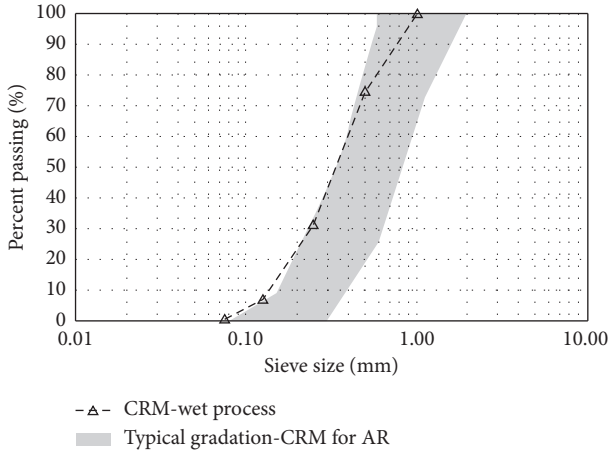

Figure 2: Gradation of crumb rubber particles.

Table 2: Passing ratio of aggregates.

Aggregate size (mm)	Passing ratio
8	100
6.3	99.5
4	71
2	28.2
1	16
0.500	12
0.250	9.2
0.125	7.1
0.063	4.4

each mixture type. As far as each kind of asphalt mixtures, volumetric properties including air voids (AVs), voids in the mineral aggregate (VMA), and voids filled with asphalt (VFA) are evaluated when numbers of gyration are 50 and 130, respectively, as shown in Table 3.

It is evident that the three asphalt mixtures were designed with similar open-graded aggregates structures due to similar VMA values for all of these three. It should be noted that the VMA value of Mix 2 was higher than the others since the additional 5% binder content is added after air voids are saturated with the binder.

4.3. Experimental Programs. Tests were carried out as per EN12697-26 using IT-CY tests by the universal testing system (UTS) to characterize the dynamic modulus of asphalt mixtures, by which the viscoelastic properties of asphalt mixtures can be defined. In this test, three cylindrical specimens were manufactured for each of the mixtures.

Figure 3 gives the load applied in the test. Notes: 1: peak load; 2: pulse repetition load; 3: rise time

Table 3: Volumetric properties of Mix ref, Mix 1, and Mix 2.

Material	Number of gyrations	AV (%)	VMA (%)	VFA (%)
Mix ref	130	21.7	31.4	30.8
Mix ref	50	24.2	33.5	27.9
Mix 1	130	1.3	34.9	96.3
Mix 1	50	2.4	35.6	93.1
Mix 2	130	3.5	44.9	92.3
Mix 2	50	4.3	45.4	90.6

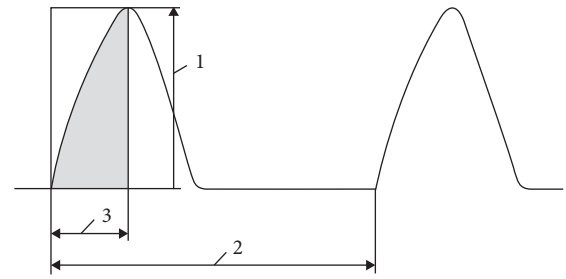

Figure 3: Load applied in the IT-CY test. (1) peak load; (2) pulse repetition load; (3) rise time.

The stiffness modulus value was obtained with the following equation:

$$E = \frac{F \times (\nu + 0.27)}{z \times h}, \tag{21}$$

in which E represents the stiffness modulus of the asphalt mixture, F represents the load applied in the IT-CY test, z represents the horizontal deformation during the test, h means the average thickness of the asphalt mixture specimen, and ν presents Poisson's ratio.

The dynamic stiffness modulus test was conducted under the indirect loading condition at 2 different temperatures (2 and 10°C) and 4 different loading frequencies (5, 3.3, 1.8, and 1.1 Hz). The test temperatures were selected according to the standard EN12697-26 and the selection of loading frequencies recommended in the control system software of the laboratory equipment. It should be noted that the tests must be conducted from the lowest temperature to the highest temperature and from the highest frequency to the lowest frequency. Stress and strain values were recorded continuously to calculate the stiffness modulus of the asphalt mixture.

4.4. Testing Results. Table 4 gives the results of the stiffness modulus as well as the

The stiffness modulus master curves were constructed by using the time-temperature superposition principle (TTSP) [35, 36]. The horizontal shift factors were calculated by the so-called Williams–Landel–Ferry (WLF) equation [37]:

$$\log \alpha_T = -\frac{C_1 \cdot (T - T_{\text{ref}})}{C_2 + (T - T_{\text{ref}})}, \tag{22}$$

where a_T represents the shift factor; C_1 and C_2 are the equation parameters, respectively; T_{ref} represents the reference temperature; and T is the testing temperature. The stiffness modulus was modeled by using the modified

Table 4: Stiffness modulus of Mix ref, Mix 1, and Mix 2.

Asphalt mixture	T_{test} (°C)	Modulus (MPa)	f (Hz)
Mix ref	2	9101	5.0
	2	8525	3.3
	2	7963	1.8
	2	6625	1.1
	10	7915	5.0
	10	7245	3.3
	10	6402	1.8
	10	5523	1.1
Mix 1	2	1995	5.0
	2	1917	3.3
	2	1765	1.8
	2	1656	1.1
	10	1705	5.0
	10	1580	3.3
	10	1332	1.8
	10	1200	1.1
Mix 2	2	1376	5.0
	2	1300	3.3
	2	1175	1.8
	2	1128	1.1
	10	1127	5.0
	10	944	3.3
	10	756	1.8
	10	671	1.1

Christensen–Anderson–Marasteanu (CAM) model [38]. Figure 4 gives the master curves of the stiffness modulus.

The master curves were developed on two replicates. Results showed an acceptable variability, with the coefficient of variation of the average between two samples below 10% for all the cases. The shift factors were optimized on the dynamic modulus master curve and were then applied to the phase angle master curve. The results provided an adequate accuracy in modeling the raw data with the R^2 coefficient being above 97% for all mixes. It can be seen that as the frequency was low (or temperature was high), Mix ref and Mix 1 showed similar stiffness modulus. However, as far as to Mix 2, it showed a lower stiffness modulus. This can be due to too much free asphalt in Mix 2 playing the role of lubricant and reducing the stiffness modulus. As the frequency was high (or temperature was low), Mix 1 and Mix 2 showed similar modulus stiffness, but both of them were lower than that of Mix ref.

5. Finite Element (FE) Modeling of the IT-CY Test

5.1. Construction of the Geometrical Model. The geometrical model is given in Figure 5.

The IT-CY test was simulated using standard SGC specimen size, with a diameter of 100 mm and a thickness of about 45 mm, measured from the results of the experimental tests. It was established for three parts, including one asphalt mixture specimen and two metal bearing blocks. The width of the bearing block is 15 mm, and the inner surface has the same arc as the specimen. The time-domain analysis was selected to perform the simulation. The time step length was

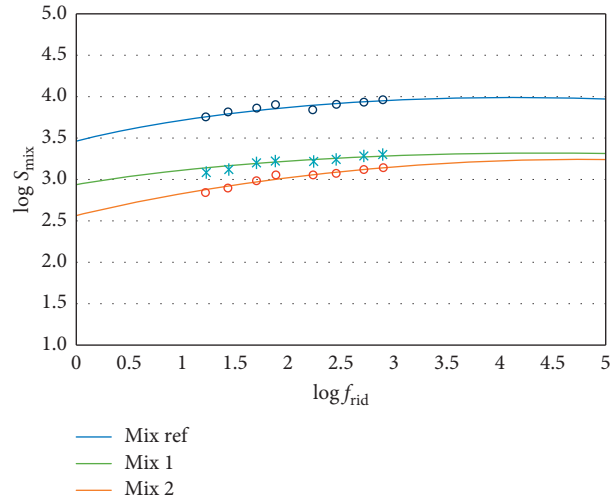

Figure 4: Stiffness modulus master curves.

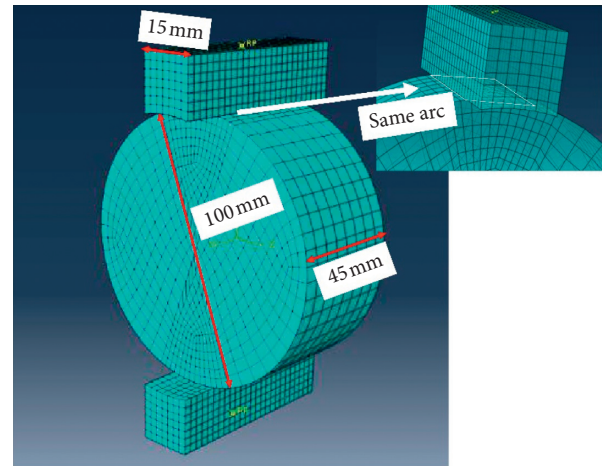

Figure 5: Schematic diagram of the geometrical model.

determined as 0.01 s to reduce the calculation time and total simulation time equaled 3 s.

5.2. Materials Properties. The more elements and parameters in a model, the more close to the real mechanical properties of viscoelastic material itself and reflecting the characteristics of viscoelastic materials at various stages. However, too many selected parameters will slow down the fitting process and its effect to improve accuracy not obvious. Based on some references, 7 parameters (E_0, E_1, E_2, E_3, η_1, η_2, and η_3) for the GMM were determined. That is to say, the GMM was consisting of 3 MM units and 1 spring in parallel connection. So, the value of m is 3, and ω_n means the reduced frequency in equation (10).

In this way, by fitting equation (10) with the least-squares method, 7 parameters characterized viscoelasticity property of asphalt mixtures will be determined. The detailed parameters of three different asphalt mixtures under 2 temperatures and 4 frequencies are shown in Table 5.

Table 5: Parameters for characterizing the GMM.

Mixes	E_0 (MPa)	E_1 (MPa)	E_2 (MPa)	E_3 (MPa)	η_1 (MPa•s)	η_2 (MPa•s)	η_3 (MPa•s)
Mix ref (2°C)	80	41	11748	8330	5283.7	58.0	1400.4
Mix 1 (2°C)	88	7620	10200	80	6822	760	688.2
Mix 2 (2°C)	84	5403	9200	183	8623	1589	236
Mix ref (10°C)	76	3705	1589	639	2566	25	10208
Mix 1 (10°C)	76	122	5689	2547	15236	1563	263
Mix 2 (10°C)	82	3563	325	1569	4896	14635	2894

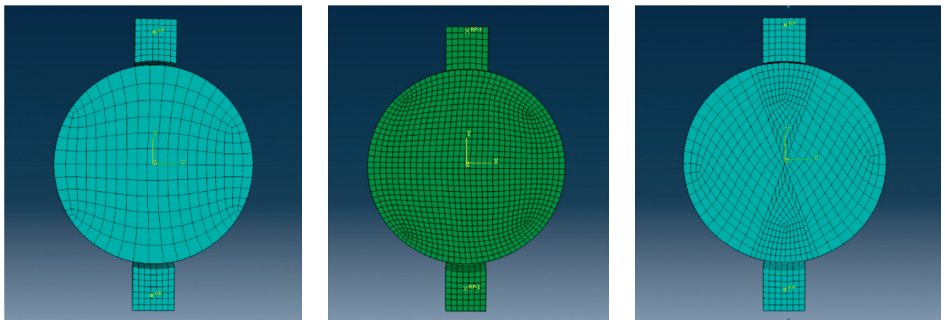

(a) (b) (c)

Figure 6: Three different meshing used in FE modeling: mesh (a), mesh (b), and mesh (c).

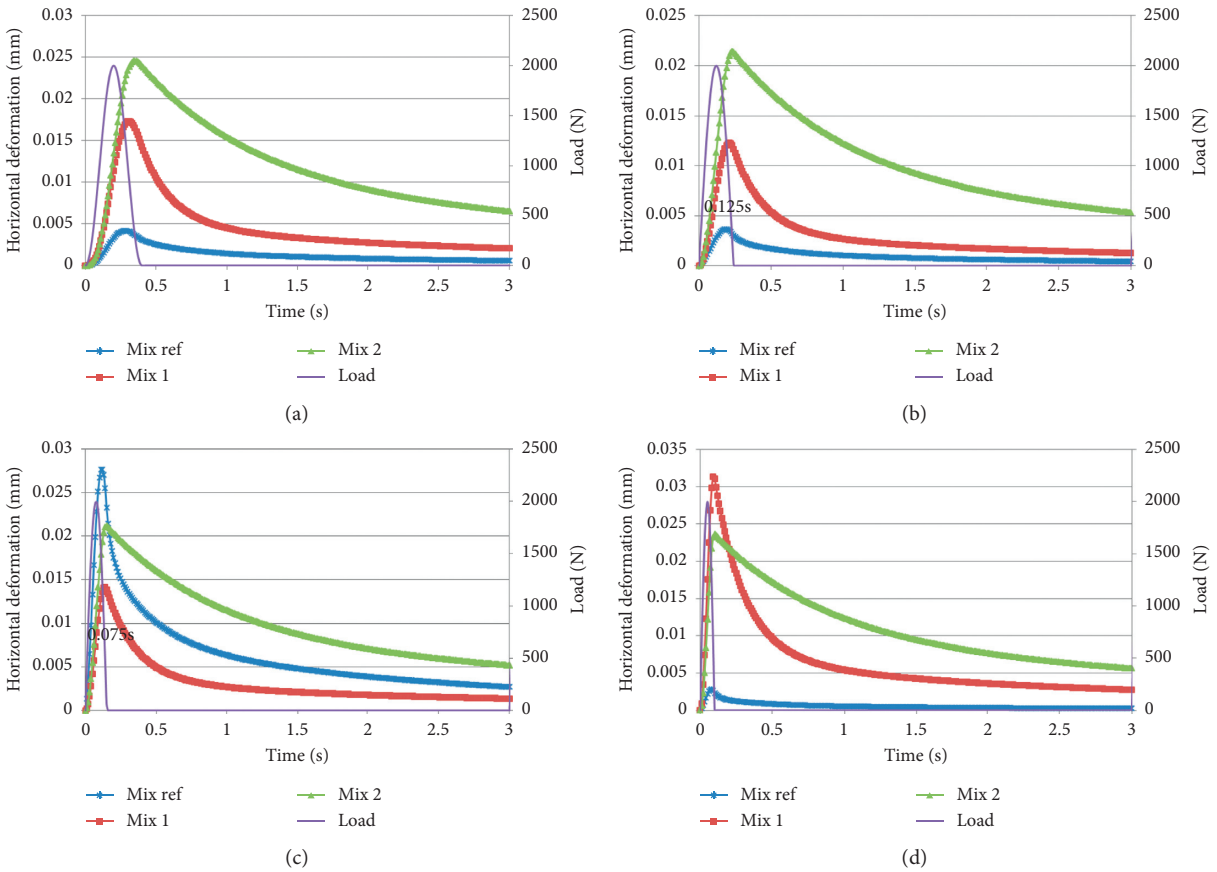

Figure 7: Simulation results: (a) $f = 1.1$ Hz; (b) $f = 1.8$ Hz; (c) $f = 3.3$ Hz; (d) $f = 5$ Hz in one cyclic.

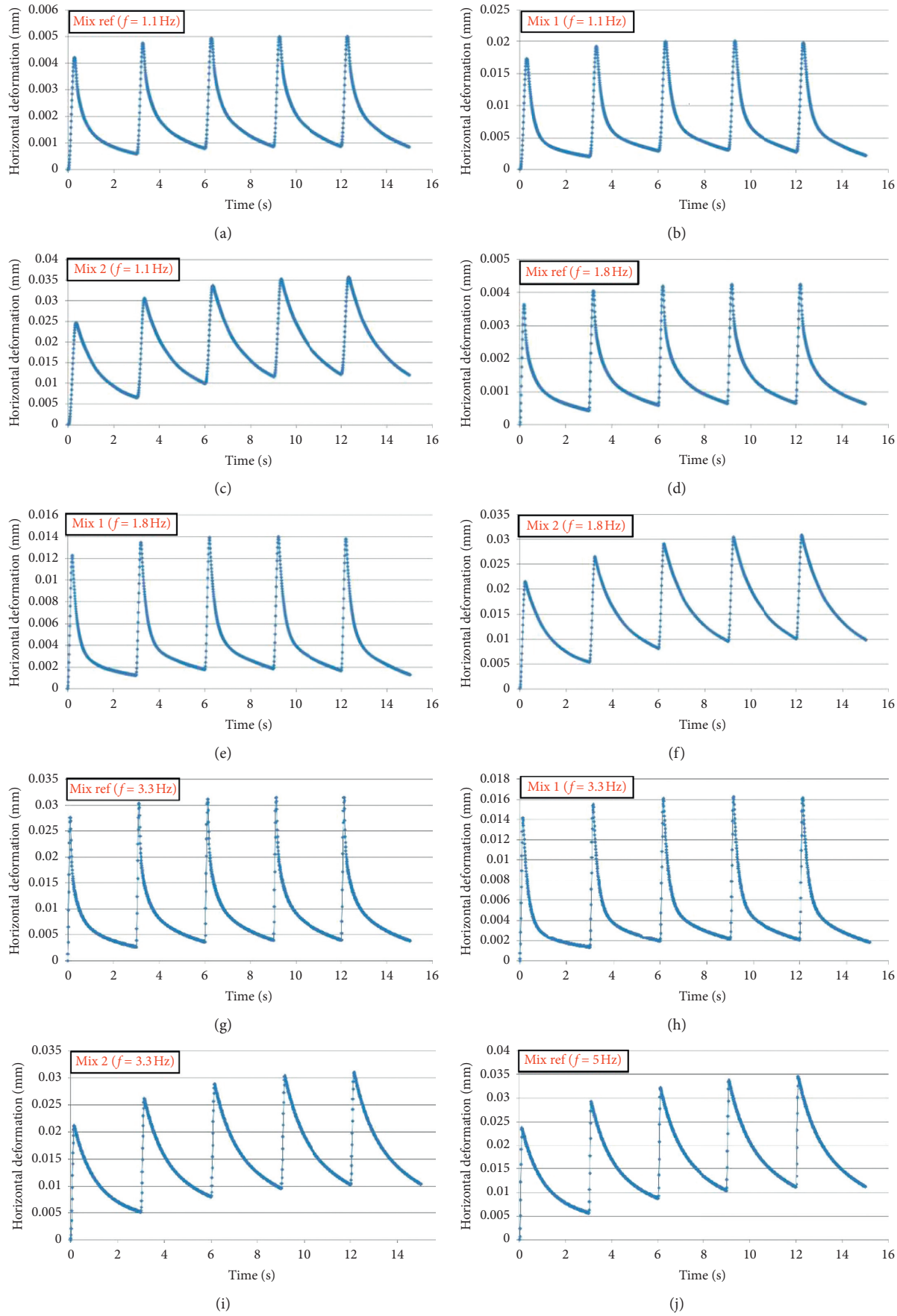

Figure 8: Continued.

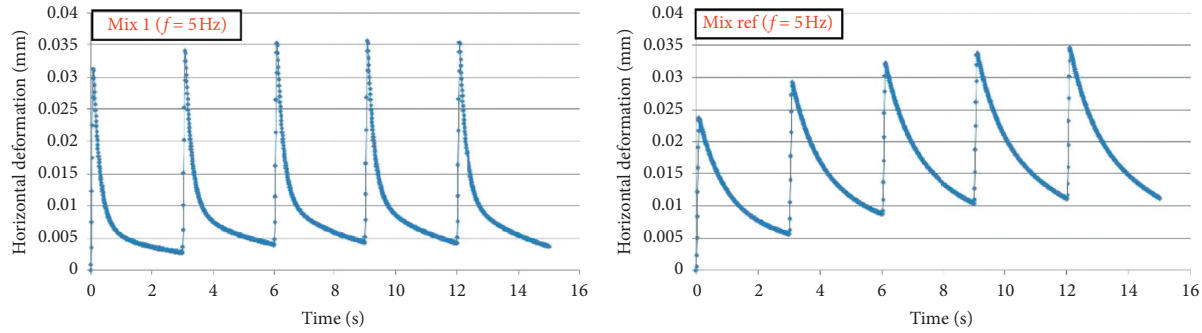

(k) (l)

Figure 8: Simulation results in five cyclic at temperature 2°C.

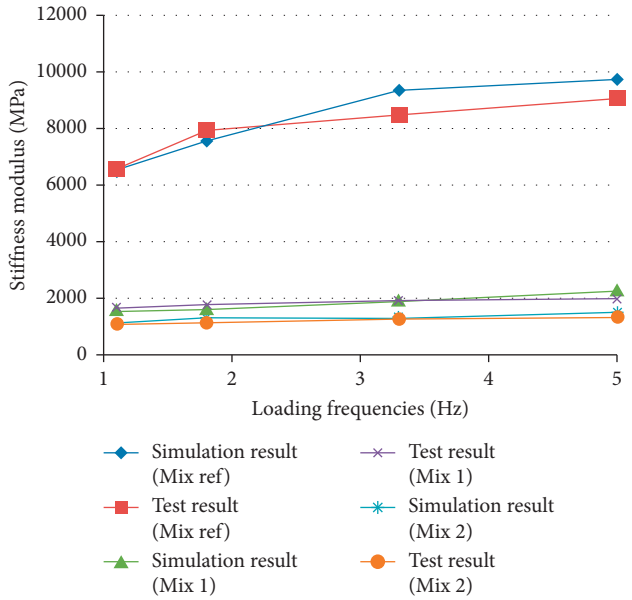

Figure 9: Comparisons between the simulation results and test results.

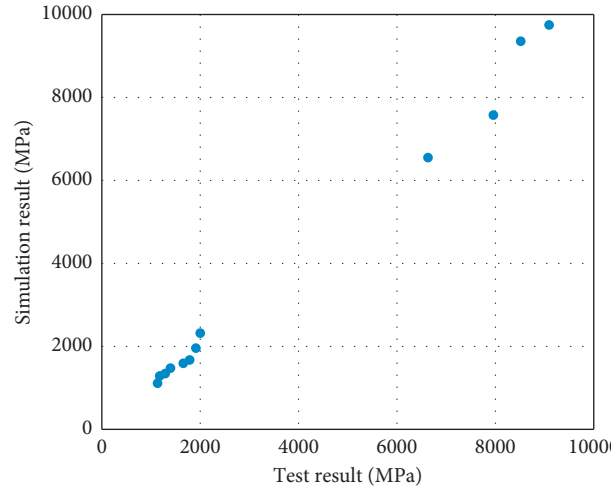

Figure 10: Test results vs. simulation results.

5.3. Finite Element Meshing. The meshes with different densities were used to compare the simulation results and to determine the convergence accuracy of the simulation, as shown in Figure 6. The grid size was determined by comparing the sizes of the sample and metal blocks. Three different grid sizes were selected by varying meshing densities.

It can be seen in Figure 6 that mesh (a) was coarse and the number of elements was minimal; thus, its computing time and storage space were relatively small, but the calculation accuracy may not be as good as the other ones. Mesh (b) was finer, and the number of elements was higher; thus, more precise calculations, more calculation time, and storage space can be foreseen. Mesh (c) was modified based on the mesh (a) and (b) with overall mesh size as same as (b), but the only partial area localized at the load was meshed more finely to prevent the local stress concentration convergence problems. However, compared with mesh (b), the computing time and storage space were much less. The results of the preliminary simulation showed that the three methods of meshing are closed to each other, but the third kind of mesh is convergent faster, consuming less computation time and less storage space, so the third kind of the meshing method is used for detailed simulation analysis. In this simulation, the rigid body in constraint was selected for metal bearing blocks. Hexahedral reduction integral element C3D8R was selected for the asphalt mixture specimen.

6. Simulation Results and Model Validations

6.1. Simulation Results. Figure 7 gives the simulation results under varying loading frequencies.

It is clearly shown that the horizontal deformations increase first and then decrease as the loading time increases, and the peak value of deformations lags behind the peak loading under the same loading cycle, which demonstrates that the digital sample behaves as a viscoelastic material under dynamic load. All horizontal deformation curves show delay trends compared with the load curve. It is known that with the same input loading frequency, more delay of the deformation demonstrates the more viscosity part accounting for total parts [39]. As can be observed in Figure 7, the comparison of the delay time is Mix 2 > Mix 1 > Mix ref,

evidencing that the much more binder content in Mix 2 improved the proportion of the viscosity part. It can be indicated that the IT-CY model based on FEM in this study is capable to characterize the macroscopic viscoelastic behaviors of asphalt mixture.

To balance the computational cost and the smoothness of the horizontal deformation response curves, 300 time-increments (computation points) were assigned for each loading cycle. The responses between horizontal deformations of point A vs. time under different loading frequencies are given in Figure 8. The abscissa represents the loading time, and the ordinate represents the deformation of the specimen in the horizontal direction. The horizontal deformation at 300 time-increments was recorded under different loading frequencies (1.1 Hz, 1.8 Hz, 3.3 Hz, and 5 Hz). The stiffness modulus can be determined as per equation (21). In this way, the stiffness modulus under different loading frequencies and temperatures can be calculated for comparison with the testing results, which are presented in the following section.

6.2. Model Validation. Figure 9 gives the comparison of stiffness modulus under different loading frequencies between the test result and the simulation result.

Good agreements are observed between these results. The difference between the simulation results and test results for Mix ref, Mix 1, and Mix 2 is calculated as 5.73%, 6.45%, and 5.03%, respectively. The differences as the loading frequency equals 1.1 Hz, 1.8 Hz, 3.3 Hz, and 5 Hz are calculated as 2.06%, 6.35%, 4.99%, and 9.57%, respectively. These differences are acceptable for the proposed FE model. The above results highlight the rationality and reliability of the proposed model to simulate the IT-CY test. Also, it is evident that a big difference can be observed for higher loading frequency. That is to say, the proposed model can be more accurate for lower loading frequency. For different asphalt mixtures, the difference between the test results and simulation results was similar. Figure 10 gives a comparison of all the stiffness modulus for the three mixtures. Similar results can be observed by the comparison. These differences are considered acceptable for the developed FE model to characterize the viscoelastic properties of DAMs.

7. Conclusions

In the present study, the research process to use FE modeling techniques to understand the mechanical behavior of DAMs in IT-CY tests was conducted. Three DAMs were designed in the laboratory, and the IT-CY tests were conducted to characterize the viscoelastic mechanical behavior, by which the reliable input material parameters for FE modeling were determined. The following are the conclusions that can be drawn from the above research process:

(i) The Prony series can be used to characterize the viscoelastic behavior of DAMs and can be determined from the IT-CY tests, by fitting the results of the GMM with the least-squares method.

(ii) The dynamic modulus master curves were typical of asphalt mixtures. During the IT-CY test, as the frequency was low (or temperature was high), Mix ref and Mix 1 showed similar stiffness modulus higher than that of Mix 2. This can be due to too much free asphalt in Mix 2 playing the role of lubricant and reducing the stiffness modulus. As the frequency was high (or temperature was low), Mix 1 and Mix 2 showed similar modulus stiffness but both of them were lower than that of Mix ref.

(iii) From the simulation results, the comparison of the delay time is Mix 2 > Mix 1 > Mix ref, evidencing that the much more binder content in Mix 2 improved the proportion of the viscosity part. It can be indicated that the IT-CY model based on FEM in this study is acceptable to characterize the viscoelastic behaviors of asphalt mixture. The longer delay time of DAMs supports what was the main scope of the mix design that is, increasing the damping response than the reference mixture, indicating a more viscous response under loading with a consequent higher energy dissipation and reduction of the vibratory mechanism.

(iv) Good agreements were noted between the simulation results and test results, demonstrating that the FE model can provide an accurate prediction of the mechanical behavior of DAMs. The proposed model can be more accurate for the lower loading frequency of the IT-CY test.

Data Availability

The experimental and modeling data used to support the findings of this study are available from the corresponding author upon request.

Conflicts of Interest

The authors declare that they have no conflicts of interest.

Acknowledgments

This research was supported by the Fundamental Research Funds for the Central Universities (2017XKQY045).

References

[1] M. Barman, M. Zaman, and S. Commuri, "Alternative analysis of indirect tensile test results for evaluating fatigue characteristics of asphalt mixes," *Construction and Building Materials*, vol. 166, pp. 204–213, 2018.

[2] T. Singh, E. Haas, and E. Wass, "Indirect tensile test (IDT) to determine asphalt mixture performance indicators during quality control testing in New Jersey," *Transportation Research Record: Journal of the Transportation Research Board*, vol. 2672, no. 28, pp. 394–403, 2018.

[3] Y. Zhao, "Accuracy improvement for two-dimensional finite-element modeling while considering asphalt mixture meso-structure characteristics in indirect tensile test simulation,"

Journal of materials in civil engineering, vol. 32, no. 10, Article ID 04020275, 2020.

[4] P. Zieliński, "Indirect tensile test as a simple method for rut resistance evaluation of asphalt mixtures–polish experience," *Road Materials and Pavement Design*, vol. 24, pp. 1–17, 2020.

[5] J. uang, J. Zhang, J. Ren, and H. Chen, "Anti-rutting performance of the damping asphalt mixtures (DAMs) made with a high content of asphalt rubber (AR)," *Construction and Building Materials*, vol. 271, Article ID 121878, 2021.

[6] J. Fu, L. Lei, X. Ma, and Z. Liu, "Experimental procedure and finite element analysis for an indirect tensile test of asphalt concrete," *Road Materials and Pavement Design*, vol. 19, no. 8, pp. 1904–1925, 2017.

[7] J. Huang and Y. Sun, "Effect of modifiers on the rutting, moisture-induced damage, and workability properties of hot mix asphalt mixtures," *Applied Sciences*, vol. 10, no. 20, p. 7145, 2020.

[8] X. King and J. Ye, "Element analysis of indirect tensile fatigue test of asphalt mixture," *Applied Sciences*, vol. 9, no. 2, p. 327, 2017.

[9] W. Liu, Y. Gao, and L. Li, "Micromechanical simulation of influence factors of indirect tensile test of asphalt mixture," *Journal of Testing and Evaluation*, vol. 46, no. 2, pp. 832–841, 2017.

[10] S. Yue, J. Zheng, D. Chen, and L. You, "Moduli decay for the asphalt mixture under different loading conditions," *Applied Sciences*, vol. 8, no. 5, p. 840, 2018.

[11] Y. Sauzéat, L. Wan, and L.-J. Sun, "Three-dimensional discrete element modelling of influence factors of indirect tensile strength of asphalt mixtures," *International Journal of Pavement Engineering*, vol. 20, no. 6, pp. 724–733, 2019.

[12] S. He, "Investigation on indirect tensile test of asphalt mixture based on the discrete element method," *Journal of Testing and Evaluation*, vol. 48, no. 3, 2020.

[13] J. Huang and Y. Huang, "Effect of modifiers on the rutting, moisture-induced damage, and workability properties of hot mix asphalt mixtures," *Applied Sciences*, vol. 10, no. 20, p. 7145, 2020.

[14] J. Huang, M. Losa, and P. Leandri, "Determining the effect of damping layers in flexible pavements on traffic induced vibrations," in *Proceedings of the Advances in Materials and Pavement Prediction: Papers from the International Conference on Advances in Materials and Pavement Performance Prediction (AM3P 2018)*, Doha, Qatar; CRC Press, April 2018.

[15] D. NapierSoranakom and R. Bonaquist, "Use of strength tests for evaluating the rut resistance of asphalt concrete," *Journal of the Association of Asphalt Paving Technologists*, vol. 71, 2002.

[16] B. Birgisson, R. Roque, and G. C. Page, "Evaluation of water damage using hot mix asphalt fracture mechanics (with discussion)," *Journal of the Association of Asphalt Paving Technologists*, vol. 72, 2003.

[17] B. Birgisson and R. Roque, "And fracture in asphalt mixtures using a boundary element approach," *Journal of Materials in Civil Engineering*, vol. 16, no. 2, pp. 116–121, 2004.

[18] Y. R. Kim and M. Momen, "Modulus testing of asphalt concrete in indirect tension mode," *Transportation Research Record: Journal of the Transportation Research Board*, vol. 1891, no. 1, pp. 163–173, 2005.

[19] A. Abbas, A. Papagiannakis, and E. A. Masad, "Micromechanical simulation of asphaltic materials using the discrete element method," *Asphalt Concrete: Simulation, Modeling, and Experimental Characterization*, vol. 31, pp. 1–11, 2006.

[20] Z.-Q. Zhang, J. Tao, and B. Yang, "Research on design parameter for high temperature performance of asphalt mixture," *China Journal of Highway and Transport*, vol. 1, pp. 23–28, 2009.

[21] M. Guo, "Effect of WMA-RAP technology on pavement performance of asphalt mixture: a state-of-the-art review," *Journal of Cleaner Production*, vol. 71, Article ID 121704, 2020.

[22] D Luo, M. Abdelsalam, and Z. Zhang, "Performance of asphalt mixtures modified with lignin fiber and glass fiber: a review," *Construction and Building Materials*, vol. 209, pp. 377–387, 2019.

[23] C. Xia, "Unified characterizing fatigue performance of rubberized asphalt mixtures subjected to different loading modes," *Journal of Cleaner Production*, vol. 279, Article ID 123740, 2020.

[24] Y. Sun, G. Li, H. Basarir et al., "Laboratory evaluation of shear strength properties for cement-based grouted coal mass," *Arabian Journal of Geosciences*, vol. 12, no. 22, p. 690, 2019.

[25] Y. Sun, G. Li, N. Zhang et al., "Development of ensemble learning models to evaluate the strength of coal-grout materials," *International Journal of Mining Science and Technology*, 2020.

[26] J. Huang, R. Alyousef, M. Suhatril et al., "Influence of porosity and cement grade on concrete mechanical properties," *Advances in Concrete Construction*, vol. 10, no. 5, pp. 393–402, 2020.

[27] J. Huang, *Rubber Modified Asphalt Pavement Layer For Noise And Vibration Absorption*, University of Florence, Florence, Italy, 2019.

[28] J. Huang and Y. Sun, "Viscoelastic analysis of the damping asphalt mixtures (DAMs) made with a high content of asphalt rubber (AR)," *Advances in Civil Engineering*, vol. 2020, pp. 1–12, 2020.

[29] S. County, *Report on the Status of Rubberized Asphalt Traffic Noise Reduction in Sacramento County*, Sacramento County and Bollard & Brennan Inc, Cleveland, OH, USA., 1999.

[30] E. V. Dave, "Graded viscoelastic approach for modeling asphalt concrete pavements," in *Proceedings of the American Institute of Physics Conference Proceedings*, pp. 736–741, Kyoto Japan, May 2008.

[31] L. Zhang, H. Ma, and T. Ma, "Modeling of dynamic modulus and phase Angle master curves of rubber modified asphalt mixture," *Materials*, vol. 12, no. 10, p. 1667, 2014.

[32] L. Shan, "Analysis of linear viscoelastic response function model for asphalt binders," *Journal of Materials in Civil Engineering*, vol. 28, no. 6, Article ID 04016010, 2016.

[33] L. Shan and N. Ren, "Criterion of viscoelastic response model for asphalt binders," *Construction and Building Materials*, vol. 113, pp. 553–560, 2016.

[34] H. Yao, "Discrete element simulation of bending beam rheometer tests for asphalt binder," *International Journal of Pavement Research & Technology*, vol. 5, no. 3, 2012.

[35] M. L. Xia and N. Tapsoba, "Validation of the time-temperature superposition principle for crack propagation in bituminous mixtures," *Materials and Structures*, vol. 46, no. 7, pp. 1075–1087, 2017.

[36] Q. T. Di Benedetto and N. Tapsoba, "Temperature superposition principle validation for bituminous mixes in the

linear and nonlinear domains," *Journal of Materials in Civil Engineering*, vol. 25, no. 9, pp. 1181–1188, 2002.

[37] J. D. Ferry, *Viscoelastic Properties of Polymers*, John Wiley & Sons, Hoboken, NJ, USA, 1980.

[38] M. Zeng, "Rheological modeling of modified asphalt binders and mixtures (with discussion)," *Journal of the Association of Asphalt Paving Technologists*, vol. 70, 2001.

[39] C. Zhang, *Viscoelastic Damping Material*, National Defence Industrial Press, Beijing, China, 2012.